

PerlDiff: Controllable Street View Synthesis Using Perspective-Layout Diffusion Models

Jinhua Zhang^{1,*} Hualian Sheng^{2,*} Sijia Cai² Bing Deng² Qiao Liang²
 Wen Li¹ Ying Fu³ Jieping Ye² Shuhang Gu^{1,†}

¹School of Computer Science and Engineering, UESTC

²Independent Researcher ³Beijing Institute of Technology

{jinhua.zjh, shenghualian.shl, cssjcai, dengbingmvp}@gmail.com
 clarencliang@foxmail.com fuying@bit.edu.cn
 {liwenbnu, jieping, shuhanggu}@gmail.com

Abstract

Controllable generation is considered a potentially vital approach to address the challenge of annotating 3D data, and the precision of such controllable generation becomes particularly imperative in the context of data production for autonomous driving. Existing methods focus on the integration of diverse generative information into controlling inputs, utilizing frameworks such as GLIGEN or ControlNet, to produce commendable outcomes in controllable generation. However, such approaches intrinsically restrict generation performance to the learning capacities of predefined network architectures. In this paper, we explore the integration of controlling information and introduce PerlDiff (**P**erspective-**L**ayout **D**iffusion **M**odels), a method for effective street view image generation that fully leverages perspective 3D geometric information. Our PerlDiff employs 3D geometric priors to guide the generation of street view images with precise object-level control within the network learning process, resulting in a more robust and controllable output. Moreover, it demonstrates superior controllability compared to alternative layout control methods. Empirical results justify that our PerlDiff markedly enhances the precision of generation on the NuScenes and KITTI datasets. Our codes and models are publicly available at <https://github.com/LabShuHangGU/PerlDiff>.

1 Introduction

The advancement of secure autonomous driving systems is fundamentally dependent on the accurate perception of the vehicle’s environment. Recently, perception utilizing Bird’s Eye View (BEV) has seen rapid progress, markedly pushing forward areas such as 3D object detection [14, 15] and BEV segmentation [41]. Nonetheless, these systems necessitate extensive datasets with high-quality 3D annotations, the acquisition of which typically involves two consecutive steps: data scene collection and subsequent labeling. Each of these steps incurs significant expenses and presents considerable challenges in terms of data acquisition.

To mitigate the issue of data scarcity, the adoption of generative technologies [5, 9, 32] has proven practical for reversing the order of data annotation. The paradigm of this approach is to use the collected annotation as controlling information to generate the corresponding lifelike images depicting urban street scenes. By implementing this strategy, it is possible to dramatically lower the costs associated with data annotation while also facilitating the generation of extensive long-tail datasets, subsequently leading to improvements in the perception model’s performance. Pioneering research,

*Equal contribution. †Corresponding author.

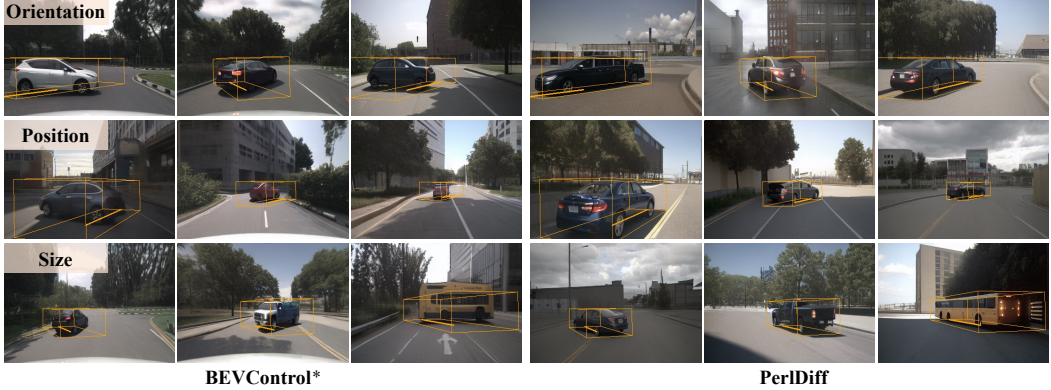


Figure 1: PerlDiff enhances controllability over BEVControl* using geometric priors. **First row:** Adjusting BEV 3D annotation yaw changes the vehicle angles in generated images. **Second row:** Shifting annotated BEV coordinates moves vehicles forward in the scene. **Third row:** Morphing the object into changing vehicle types such as a car, a truck, and a bus increases the object size.

exemplified by BEVGen [30], harnesses the capabilities of autoregressive transformers [5, 32] to render detailed visualizations of street scenes. Additionally, subsequent studies such as BEVControl [38] and MagicDrive [6] employ diffusion-based techniques, including GLIGEN [13] and ControlNet [39], to integrate controlling information through a basic cross-attention mechanism. However, these methods simply extract integrated conditional features from controlling information to adjust the generation process and are limited in making full use of detailed geometric layout information for accurate attention map manipulation. While these techniques make strides towards meeting the requirements for generating 3D annotations, Fig. 1 demonstrates that there remains significant potential for improvement in object controllability.

To this end, in this paper, we introduce the perspective-layout diffusion models (PerlDiff), a novel method specifically designed to enable precise control over street view image generation at the object level. In addition to extracting integrated conditional features from controlling condition information, *i.e.* 3D annotations, our PerlDiff model explicitly renders perspective layout masking maps as geometric priors. Subsequently, a Perl-based controlling module (Perl-CM) is proposed to leverage the geometric priors, *i.e.* perspective layout masking maps. Within Perl-CM, an innovative Perl-based cross-attention mechanism is utilized to accurately guide the generation of each object with their corresponding condition information. We integrate Perl-CM into the pre-trained Stable Diffusion model [24] and fine-tune it on our training dataset. Consequently, our PerlDiff incorporates the formidable generative capabilities of Stable Diffusion with the finely detailed geometric priors of perspective layouts, effectively harnessing their respective strengths for precise object-level image synthesis. Overall, our PerlDiff is capable of generating precise, controllable street view images while also maintaining high fidelity (see Section 3 for details).

The main contributions of this paper are summarized as following three-folds: **(i)** We present PerlDiff, a newly developed framework crafted to synthesize street view images from user-defined 3D annotations. Our PerlDiff carefully orchestrates the image generation process at the object level by leveraging perspective layout masks as geometric priors. **(ii)** We propose a Perl-based cross-attention mechanism that utilizes perspective layout masking maps from 3D annotations to enhance the underlying cross-attention mechanism within Perl-CM. This method enables precise control over the street view image generation process by integrating road geometry and object-specific information derived from BEV annotations. **(iii)** Our PerlDiff method attains state-of-the-art performance on the NuScenes [1] and KITTI [7] dataset compared to existing methods, markedly enhancing detection and segmentation outcomes for synthetic street view images. Furthermore, it holds the potential to function as a robust traffic simulator in the future.

2 Related Work

Diffusion-based Generative Models in Image Synthesis. Initially developed as a method for modeling data distributions through a sequence of Markov chain diffusion steps [26, 28, 29], diffusion models have undergone rapid advancement. Ho et al. [9] introduced denoising diffusion

probabilistic models (DDPMs), which have established new benchmarks in the quality of image synthesis. Following efforts have aimed to enhance the efficiency and output diversity of these models by investigating various conditioning strategies [2, 4], architectural adjustments, and training methodologies to refine the image synthesis process [11]. Nichol and Dhariwal [4] proved that diffusion models can be text-conditioned to produce coherent images that are contextually appropriate. Furthermore, advances such as multimodal-conditioned diffusion models have effectively utilized layout images [13, 22, 24, 39], semantic segmentation maps [13, 39], object sketches [13, 19, 33, 39], and depth maps [13, 19, 39] to inform the generative process. These methods enable more targeted manipulation of the imagery, thus yielding complex scenes characterized by enhanced structural integrity and contextual pertinence.

Data Generation for Autonomous Driving. BEVGen [30] represents the pioneering endeavor to harness an autoregressive Transformer [5, 32] for synthesizing multi-view images pertinent to autonomous driving. Building upon this, BEVControl [38] introduces a novel method that incorporates a diffusion model [9] for street view image generation, and integrates cross-view attention mechanisms to maintain spatial coherence across neighboring camera views. Subsequently, MagicDrive [6] propels the field forward by refining the method for controlling input conditions, drawing insights from ControlNet [39]. DrivingDiffusion [12] further augments the framework by introducing a consistency loss designed to achieve the perceptual uniformity requisite for high precision in the generation of video from autonomous driving. Panacea [36] broadens the capabilities of the model by tackling the challenge of ensuring temporal consistency in video. In contrast to the above approaches, which primarily utilize controlling input conditions to steer the image generation process, our PerlDiff exploits detailed geometric layout information from the input to directly guide object generation with higher precision.

Geometric Constraints in Image Generation. Incorporating geometric priors into image synthesis has been explored to a lesser extent. Work on 3D-aware image generation [20, 21] suggests the feasibility of integrating geometric information into generative processes to improve spatial coherence. Nevertheless, these methods often rely on complex 3D representations and may not be directly applied to diffusion model frameworks. Recently, BoxDiff [37] reveals a spatial correspondence between the attention map produced by the diffusion model and the corresponding generated image. During the testing phase, the geometric configuration of the attention map’s response values is adjusted to yield a more precise image generation. ZestGuide [3] introduces a loss function that enforces a geometric projection onto the attention map, further refining the shape of the attention map’s response values to closely approximate the geometric projection of the control information during the inference stage. However, utilizing text prompts to facilitate the generation of complex urban environment layouts poses inherent challenges, owing to the need for crafting intricate prompts to accurately depict urban environments. Furthermore, modifying the cross-attention map to impose strict constraints during the denoising phase of inference can disrupt the intrinsic relationships, leading to a suboptimal approach to synthesizing controllable images. In contrast, our PerlDiff incorporates geometric prerequisites as training priors to guide the generation of street view images, offering a more effective solution.

3 Controllable Street View Generation Based on Perspective Layout

In this paper, we introduce PerlDiff, depicted in Fig. 2, which is designed to enable controllable multi-view street scene generation using BEV annotations. Specifically, PerlDiff leverages perspective projection information from BEV annotations as controlling condition within the training regimen and utilizes perspective layout masks as geometric priors, enabling accurate guidance in object generation. In the following sections, we delineate the process of encoding the controlling condition information from the BEV annotations in Section 3.1. Additionally, we explain how incorporating perspective layout knowledge ensures object controllability in street view image generation in Section 3.2.

3.1 Controlling Conditions Encoding

Given BEV annotations of a street scene, our goal is to generate multi-view street images. To be more specific, for controllable street view image generation, we extract not only scene information (*i.e.*, textual scene descriptions S_d and street maps M revealing features such as road markings and obstacles) but also object information (*i.e.*, bounding box parameters P and the associated object category Y) from BEV annotations as controlling conditions. These controlling conditions encompass

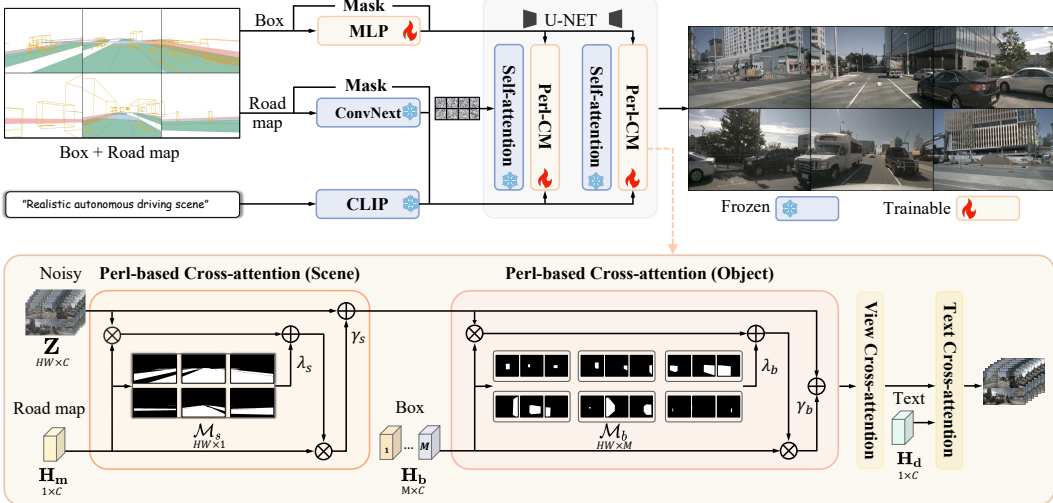


Figure 2: Overview of **PerlDiff** framework for multi-view street image generation. our PerlDiff utilizes perspective layout masking maps derived from BEV annotations to integrate scene information and object bounding boxes. **Perl-CM** is responsible for integrating control information through employing **Perl-based cross-attention (Scene & Object)** mechanism, using Perl masking map (road & box) as geometric priors to guide object-level image generation with high precision. View cross-attention ensures consistency across multiple views, while Text cross-attention integrates textual scene descriptions to facilitate further adjustments.

rich semantic and geometric information, so establishing a robust encoding method to utilize this information is essential for generating street view images. Hereafter, we present our controlling condition encoding approach. We omit the details of multi-view perspectives for notational simplicity.

Perl Scene Information encompasses perspective scene images and supplemental data specific for the whole scene. Typically, the selected scene for annotation is coupled with a street map of the driving environment, which visually differentiates between the road and other background elements using distinct colors. In addition, a generic textual description of the scene is customizable to align with particular scenarios. We employ ConvNext [16] and the CLIP text encoder [23] to encode the perspective road map, denoted as \mathbf{S}_m , derived from the projection of the street map and the textual scene description \mathbf{S}_d , respectively. This approach results in the generation of encoded scene features $\mathbf{H}_m \in \mathbb{R}^{1 \times C}$ for the road map and $\mathbf{H}_d \in \mathbb{R}^{1 \times C}$ for the textual scene description:

$$\mathbf{H}_m = \text{ConvNext}(\mathbf{S}_m), \quad \mathbf{H}_d = \varphi(\mathbf{S}_d). \quad (1)$$

Perl Object Information encapsulates perspective geometric data alongside object category information, which stems from the projections of annotated BEV 3D boxes. This element plays a pivotal role in enabling inverse 3D labeling. Through projecting BEV 3D annotations onto their corresponding perspective images, we ascertain eight 2D corner points for each bounding box within a single image, denoted as $\mathbf{P}_g \in \mathbb{R}^{M \times 2 \times 8}$, where M represents the maximum number of bounding boxes and eight corresponds to the number of corners per bounding box. In conjunction with the object’s categorical text $\mathbf{P}_c = \{\mathbf{P}_{c_i}\}_{i=1}^M$, we derive the encoded box geometric features $\mathbf{H}_g \in \mathbb{R}^{M \times C}$ and the box categorical features $\mathbf{H}_c \in \mathbb{R}^{M \times C}$, which are illustrated as follows:

$$\mathbf{H}_g = \mathcal{F}(\mathbf{P}_g), \quad \mathbf{H}_c = \varphi(\mathbf{P}_c), \quad (2)$$

where $\mathcal{F}(\cdot)$ is the Fourier embedding [18] function, $\varphi(\cdot)$ represents the pre-trained text embedding encoder of CLIP [23] and C representing the dimension of features. Furthermore, we concatenate the encoded geometric features \mathbf{H}_g and categorical features \mathbf{H}_c and subsequently pass the concatenated vector through a Multilayer Perceptron (MLP) [31] \mathbf{F} , to achieve feature fusion $\mathbf{H}_b \in \mathbb{R}^{M \times C}$. The resulting fused box feature representation is given by:

$$\mathbf{H}_b = \mathbf{F}([\mathbf{H}_g, \mathbf{H}_c]). \quad (3)$$

We subsequently input the encoded conditions into the denoising diffusion model to guide the generation process. This is achieved utilizing Perl-based cross-attention mechanism that incorporates Perl masking maps, as detailed below.



Figure 3: Visualization of cross-attention maps reveals perceptual congruency with the generated image. BEVControl* produces disorganized and vague attention maps, which result in inferior image quality. Conversely, our PerlDiff method fine-tunes the response within the attention maps, resulting in more accurate control information at the object level and improved image quality. See more qualitative examples in the Appendix D.

3.2 Object Controllability via Perl-based Controlling Module

Perl-based Controlling Module (Perl-CM) is responsible for integrating controlling condition information, which encompasses both the Perl scene and object information, into the latent feature maps of noisy street view images. This integration is primarily achieved via the scene and object Perl-based cross-attention mechanism. Initially, this mechanism assigns initial values to the attention maps, under the guidance of road and box Perl masking maps. Throughout the training of the network, these values are optimized to ensure that the response of the attention map accurately corresponds to the regions where the objects are located. Subsequently, the information from both the road map and the bounding box are sequentially integrated into the noisy street view image. To more effectively integrate Perl scene and object information, a gating operation is used, similar to the method employed in GLIGEN [13], which dynamically adjusts the contribution of condition information according to the adaptive process. To ensure multi-view consistency, View Cross-attention leverages information from the immediate left and right views for uniformity across various perspectives. Additionally, Text Cross-attention manipulates the weather and lighting conditions of street scenes using textual scene description. The details of the Perl-CM process are delineated in the Algo. 1.

Perl Masking Map (road & box) is comprised of Perl road masking map $\mathcal{M}_s \in \mathbb{R}^{HW \times 1}$ and Perl box masking map $\mathcal{M}_b \in \mathbb{R}^{HW \times M}$, where H and W represent the height and width dimensions of the image, respectively. These masking maps are articulated as follows:

$$\mathcal{M}_s = \Upsilon(\mathbf{S}_m), \quad \mathcal{M}_b = \Phi(\mathbf{P}_g), \quad (4)$$

where $\Upsilon(\cdot)$ generates the masking map for the non-empty regions of the projected road maps. Meanwhile, $\Phi(\cdot)$ produces the masking map corresponding to the inner region of each projected 3D bounding box for every perspective image, enabling precise control at the object level.

Perl-based Cross-attention (Scene & Object) leverages the prior masking maps to enhance the learning of cross-attention between the input controlling conditions and the noisy street view images. As depicted in Fig. 3, the cross-attention map exhibits perceptual equivalence with the generated street view image. However, this correspondence is imprecise and lacks the necessary alignment during the training stage. To this end, our approach utilizes a Perl-based cross-attention mechanism that incorporates geometric knowledge derived from both the scene context and the bounding box into the computation of the cross-attention map. In PerlDiff, the road map and object bounding box data are seamlessly merged with the noisy street view images throughout each stage of the denoising process. For the sake of notational simplicity, the linear embeddings and normalization steps typically involved in the attention mechanism have been omitted.

$$\mathcal{A}_s = \text{softmax}(\lambda_s \cdot \mathcal{M}_s + \mathbf{Z} \mathbf{H}_m^T / \sqrt{d}), \quad \mathcal{A}_b = \text{softmax}(\lambda_b \cdot \mathcal{M}_b + \mathbf{Z} \mathbf{H}_b^T / \sqrt{d}) \quad (5)$$

where λ_s and λ_b are weight parameters that control the influence of the masking map, d denotes the dimensionality, and $\mathbf{Z} \in \mathbb{R}^{HW \times C}$ is the noisy street view image. Here, $\mathcal{A}_s \in \mathbb{R}^{HW \times 1}$ characterizes the association between the road map and the noisy image, while $\mathcal{A}_b \in \mathbb{R}^{HW \times M}$ clarifies the relationship between the conditions of the object bounding box and the noisy image. The final noisy street view image is synthesized through an attention-based aggregation mechanism enhanced by a residual connection, which can be expressed as:

$$\mathbf{Z} = \gamma_s \cdot \mathcal{A}_s \mathbf{H}_m + \mathbf{Z}, \quad \mathbf{Z} = \gamma_b \cdot \mathcal{A}_b \mathbf{H}_b + \mathbf{Z}, \quad (6)$$

Algorithm 1 Perl-based Controlling Module (Perl-CM)

Input: road map features $\mathbf{H}_m \in \mathbb{R}^{1 \times C}$, road masking map $\mathcal{M}_s \in \mathbb{R}^{HW \times 1}$, box features $\mathbf{H}_b \in \mathbb{R}^{M \times C}$, box masking map $\mathcal{M}_b \in \mathbb{R}^{HW \times M}$, scene text description features $\mathbf{H}_d \in \mathbb{R}^{1 \times C}$, noisy multi-view street image feature $\mathbf{Z} \in \mathbb{R}^{HW \times C}$, and dimension d (omit the detail of multi-view perspectives)

Output: Updated \mathbf{Z}

- 1: $\mathcal{A}_s \leftarrow \text{softmax}(\lambda_s \cdot \mathcal{M}_s + \mathbf{Z}\mathbf{H}_m^T / \sqrt{d})$
// compute attention map for the road map in perl-based cross-attention (scene)
- 2: $\mathbf{Z} \leftarrow \gamma_s \cdot \mathcal{A}_s \mathbf{H}_m + \mathbf{Z}$
- 3: $\mathcal{A}_b \leftarrow \text{softmax}(\lambda_b \cdot \mathcal{M}_b + \mathbf{Z}\mathbf{H}_b^T / \sqrt{d})$
// compute attention map for the box in perl-based cross-attention (object)
- 4: $\mathbf{Z} \leftarrow \gamma_b \cdot \mathcal{A}_b \mathbf{H}_b + \mathbf{Z}$
- 5: $\mathbf{Z} \leftarrow \mathbf{Z}_{in} + \mathcal{C}(\mathbf{Z}_{in}, \mathbf{Z}_l, \mathbf{Z}_l) + \mathcal{C}(\mathbf{Z}_{in}, \mathbf{Z}_r, \mathbf{Z}_r)$
// maintain visual consistency via view cross-attention
- 6: $\mathbf{Z} \leftarrow \text{softmax}(\mathbf{Z}\mathbf{H}_d^T / \sqrt{d}) \mathbf{H}_d + \mathbf{Z}$
// alter illumination and atmospheric effects by text cross-attention



Figure 4: Qualitative visualization on NuScenes [1] demonstrating the effects of Text Cross-attention. From left to right: *day*, *night*, and *rain* scenarios synthesized by PerlDiff, highlighting its adaptability to different lighting and weather conditions. For more examples, see the Appendix D.

where γ_s and γ_b represent learnable parameters modulating the influence of the respective conditions.

View Cross-attention is corroborated by preliminary works such as BEVControl [38], MagicDrive [6], DrivingDiffusion [12], and Panacea [36], plays an instrumental role in facilitating the synthesis of images that maintain visual consistency across varying camera perspectives. For additional information, please see the Appendix C.3.

Text Cross-attention enhances the Stable Diffusion [24] model’s ability to modulate street scenes through textual scene description. This capability is crucial for dynamically adapting the rendering of street scenes to accommodate various lighting and weather conditions. By integrating detailed textual scene description, our PerlDiff can effectively alter visual elements such as illumination and atmospheric effects, ensuring that the generated images reflect the specified conditions accurately. Please refer to Fig. 4 for qualitative examples of this enhancement.

3.3 Discussion

In contrast to previous approaches for autonomous driving such as BEVControl [38], MagicDrive [6], DrivingDiffusion [12], and Panacea [36], which employ a basic cross-attention mechanism to integrate controlling condition information, our PerlDiff leverages geometric priors via Perl masking map. This approach directs the generation of each object with its respective control information during the training phase, effectively countering the common misalignment between the attention map and condition information that often results in compromised image controllability. For instance, the attention map of BEVControl [38], illustrated in Fig. 3, demonstrates disorganized patterns and lacks precision. Conversely, our PerlDiff markedly enhances the accuracy of generated images and the granularity of condition information at the object level by ensuring meticulous guidance within the attention map. For more qualitative results, please see the Appendix D.

4 Experiments

We assess PerlDiff’s ability to control quality across multiple benchmarks, including multi-view 3D object detection, BEV segmentation and monocular 3D object detection. Subsequently, we conduct ablation studies to ascertain the contribution of each component within our proposed methodology.

Table 1: Comparison of the controllability of street view image generation on NuScenes [1] *validation* set. Our replication of BEVControl*, serving as the baseline, employs standard cross-attention mechanisms contrary to Perl-based cross-attention utilized in our PerlDiff. Outcomes demonstrating superior performance are highlighted in **bold**.

Method	Detector	FID \downarrow	mAP \uparrow	NDS \uparrow	mAOE \downarrow	Road mIoU \uparrow	Vehicle mIoU \uparrow
Oracle	BEVFormer	–	27.06	41.89	0.54	70.35	33.36
Oracle	BEVFusion	–	35.54	41.20	0.56	70.46	35.86
MagicDrive [6]	BEVFusion	16.20	12.30	23.32	–	61.05	27.01
BEVControl*	BEVFusion	23.89	9.98	19.61	0.94	60.74	22.47
PerlDiff (Ours)	BEVFusion	25.06	15.24	24.05	0.78	61.26	27.13
BEVGen [30]	–	25.54	–	–	–	50.20	5.89
BEVControl [38]	BEVFormer	24.85	19.64	28.68	0.78	60.80	26.86
BEVControl*	BEVFormer	23.89	16.48	28.08	0.88	60.74	22.47
PerlDiff (Ours)	BEVFormer	25.06	25.10	36.24	0.72	61.26	27.13

Table 2: Controllability comparison on KITTI [7] *validation* set, showcasing vehicle mAP obtained by MonoFlex [40] using data generated by our PerlDiff and the baseline BEVControl*. “NuScenes → KITTI” denotes initial training on NuScenes *train* set followed by fine-tuning on KITTI *train* set.

Method	KITTI				NuScenes → KITTI			
	Easy \uparrow	Mod. \uparrow	Hard \uparrow	FID \downarrow	Easy \uparrow	Mod. \uparrow	Hard \uparrow	FID \downarrow
Oracle	22.29	15.54	13.38	–	22.29	15.54	13.38	–
BEVControl*	0.33	0.29	0.39	39.47	1.32	1.51	1.64	32.96
PerlDiff (Ours)	11.04	7.44	6.03	39.03	13.12	9.24	7.59	31.70

4.1 Datasets

NuScenes [1] dataset comprises 1,000 urban street scenes, traditionally segmented into 700 for training, 150 for validation, and 150 for testing. Each scene features six high-resolution images (900×1600), which together provide a complete 360-degree panoramic view of the surroundings. Additionally, NuScenes includes comprehensive road maps of the driving environment, featuring details such as lane markings and obstacles. We extend the class and road type annotations similar to MagicDrive [6] and NuScenes, incorporating ten object classes and eight road types for map rendering. To address the resolution limitations of the U-Net architecture in Stable Diffusion [25], we adopt image resolutions of 256×384 as in BEVFormer [14], and 256×704 following BEVFusion [15].

KITTI [7] dataset contains 3,712 images for training and 3,769 images for validation. KITTI dataset has only one perspective image and does not have road map information. Given the varied image resolutions in KITTI (approximately 375×1242), we pad them to 384×1280 for generative learning.

4.2 Main Results

In this subsection, we assess our PerlDiff’s generative quality through the perception results of several pre-trained methods: BEVFormer [14], BEVFusion [15], and StreamPETR [34] for multi-view 3D detection; CVT [41] for BEV segmentation; all trained on the NuScenes set, and MonoFlex [40] for monocular 3D detection trained on the KITTI set. Additionally, we leverage our synthesized dataset to enhance the performance of various 3D detection models (*i.e.*, BEVFormer and StreamPETR) on the NuScenes *test* set, validating the effectiveness of our PerlDiff.

Controllable Generation on NuScenes. To evaluate the effectiveness of our PerlDiff, we trained the model on NuScenes *train* set and subsequently generated a synthetic *validation* set using the provided road maps and 3D annotations. The controllability of PerlDiff was examined by deploying perception models, originally trained on the actual *train* set, onto our synthetic *validation* set. As summarized in Tab. 1, our PerlDiff outperforms competing methods on most metrics, as tested with BEVFormer [14] and BEVFusion [15]. In a rigorous comparison, we replicated BEVControl [38] using identical settings, with the exception of our innovative element: the Perl-based cross-attention mechanism. Our PerlDiff demonstrates notable improvements, with increments of 8.62%, 8.16% and 0.16% in

Table 3: Performance comparison for the boosting performance of 3D detection models using synthesized dataset on NuScenes [1] *test* set using BEVFormer [14] and StreamPETR [34]. The “*train + Real val*” configuration serves as a benchmark, representing the ideal upper performance limit achievable. “*Syn. val*” represents the synthetic *validation* set generated by BEVControl. The numbers in parentheses indicate the performance disparity relative to the “*train + Real val*” configuration.

Training	Detector	mAP↑	NDS↑	mATE↓	mASE↓	mAOE↓
<i>train</i>	BEVFormer	28.97	42.52	72.90	28.15	56.34
<i>train + Real val</i>		32.20	45.44	69.43	27.40	52.88
<i>train + Syn. val*</i>		29.92 (-2.28%)	43.20 (-2.24%)	70.76 (+1.33%)	27.69 (+0.29%)	57.57 (+4.69%)
<i>train + Syn. val (Ours)</i>		31.66 (-0.54%)	44.91 (-0.53%)	70.09 (+0.66%)	27.56 (+0.16%)	55.05 (+2.17%)
<i>train</i>	StreamPETR	47.84	56.66	55.91	25.81	47.40
<i>train + Real val</i>		50.92	58.68	54.36	25.12	45.36
<i>train + Syn. val*</i>		47.37 (-3.55%)	56.40 (-2.28%)	56.99 (+2.63%)	25.58 (+0.46%)	47.69 (+2.33%)
<i>train + Syn. val (Ours)</i>		49.07 (-1.85%)	57.92 (-0.76%)	55.71 (+1.35%)	25.57 (+0.45%)	47.08 (+1.72%)



Figure 5: Qualitative visualization comparison on KITTI [7]. Red markers denote instances where BEVControl* inaccurately generates output compared to PerlDiff and ground truth.

the mean Average Precision (mAP), NuScenes detection score (NDS) and mean average orientation error (mAOE), respectively, compared to BEVControl* when using BEVFormer. With BEVFusion, it achieves gains of 5.26%, 4.44% and 0.16% in these metrics against BEVControl*, confirming its effectiveness at a resolution of 256×384 . The superiority of our PerlDiff is further affirmed by BEV segmentation [41] metrics, significantly outperforming BEVControl* with a 0.52% increase in Road mIoU and a 4.66% increase in Vehicle mIoU, validating the potency of the Perl-based cross-attention mechanism in improving the controllability of the scene.

Compared to the state-of-the-art MagicDrive [6], our method lags only in the FID (Fréchet Inception Distance) metric [8]. Despite this, prioritizing definitive control over generative images is crucial to their practical application in the real world. For perception models, excessive similarity in synthetic output can lead to data redundancy. our PerlDiff skillfully ensures a balance within the synthesized data spectrum, as reflected by its FID scores comparable to BEVControl*, positioning our framework as a prime choice for enhancing conditional diffusion models.

Controllable Generation on KITTI. The scarcity of training data in KITTI [7] often hampers a generative model’s capacity to discern the association between control information and the synthesis of images. To mitigate this limitation, we employ two distinct strategies for generating images within the KITTI framework: one strategy is direct training utilizing the KITTI *train* set, and the other involves preliminary training on the NuScenes *train* set with subsequent fine-tuning on the KITTI *train* set. In Tab. 2, we present the results of monocular 3D object detection on KITTI *validation* set, utilizing a pretrained MonoFlex [40] detector. In particular, BEVControl* shows substantially reduced detection efficacy with few training samples. In contrast, our PerlDiff maintains a consistently high level of data annotation performance, outperforming BEVControl* by a considerable margin. Thus, our model exhibits pronounced superiority in scenarios involving datasets with limited sizes. The visual comparison between BEVControl* and our PerlDiff is presented in Fig. 5. More visual results on KITTI can be found in the Appendix D.

Boosting Perception Models Using Synthesized Dataset. Generative models have become widely acknowledged as effective tools for data augmentation, thereby improving the generalization capabilities of perception models. To evaluate this approach, we leverage our synthesized dataset to improve the performance of various detection models on NuScenes *test* set. The gains presented in the second row of Tab. 3 confirm that augmenting with data annotated optimally (*i.e.*, using the combined real NuScenes *train + Real val* set) is beneficial. In particular, the performance of BEVFormer [14] and StreamPETR [34] improved significantly after the dataset was augmented with real *validation* set. The most notable gains for BEVFormer were observed in the mAP and NDS metrics, which increased

Table 4: Ablation of the Perl-based cross-attention mechanism, reporting 3D object detection improvements using BEVFormer [14] and BEV segmentation enhancements using CVT [41]. Numbers in parentheses indicate performance gains over the baseline.

Method	Road Mask	Box Mask	FID \downarrow	mAP \uparrow	NDS \uparrow	mAOE \downarrow	Road mIoU \uparrow	Vehicle mIoU \uparrow
Oracle			-	27.06	41.89	0.54	70.35	33.36
(a)			23.89	16.48	28.08	0.88	60.74	22.47
(b)	✓		23.83	16.27	28.40	0.86	61.18	23.14
(c)		✓	24.47	26.07	36.07	0.74	61.21	26.27
(d)	✓	✓	25.06	25.10 (+8.62%)	36.24 (+8.16%)	0.72 (-0.16%)	61.26 (+0.52%)	27.13 (+4.66%)

Table 5: Ablation of different values of masking map weight coefficients λ_s and λ_b . We report the 3D object detection results based on BEVFormer [14] and BEV Segmentation results based on CVT [41].

Method	λ_s	λ_b	FID \downarrow	mAP \uparrow	NDS \uparrow	mAOE \downarrow	Road mIoU \uparrow	Vehicle mIoU \uparrow
Oracle	-	-	-	27.06	41.89	0.54	70.35	33.36
(a)	1.0	1.0	22.37	22.30	34.08	0.73	61.31	25.03
(b)	3.0	3.0	24.88	24.41	35.75	0.74	60.58	26.82
(c)	5.0	5.0	25.06	25.10	36.24	0.72	61.26	27.13

by 3.23% and 2.92%, respectively. Similarly, for StreamPETR, increases in mAP and NDS were recorded at 3.08% and 2.02%, respectively.

Furthermore, augmentations using synthetic *validation* set yielded competitive improvements that almost matched the performance gains observed with real *validation* set. The gaps in performance metrics, such as mAP, NDS, and mAOE, were minimal, thus solidifying the value of synthetic augmentation compared to the *train-only* baseline. Specifically, BEVFormer [14] and StreamPETR [34] exhibited only slight gaps in mAP (0.54% and 1.85%), NDS (0.53% and 0.76%) and mAOE (2.17% and 1.72%), respectively. In addition, these discrepancies were even less pronounced compared to BEVControl*, highlighting the effectiveness of the Perl-based cross-attention mechanism.

4.3 Ablation Study

To determine the effectiveness of the fundamental components within our PerlDiff, we perform ablation studies concentrated on key elements: Perl-based cross-attention.

Effectiveness of Perl-based Cross-attention. To illustrate the impact of Perl-based cross-attention, we devised a comprehensive comparative experiment, the results of which are presented in Tab. 4. Method (a) employs road map and 3D box as conditions, which are integrated into the model using standard cross-attention [6, 38] with the configuration mirroring that of BEVControl*. “Box Mask” and “Road Mask” denote the process wherein the control information is merged with the model through Perl-based cross-attention. Method (a)→(b) signifies the adoption of Perl-based cross-attention for the road map, leading to improvements of 0.44% in Road mIoU and 0.32% in NDS. These gains underscore the augmented controllability achieved by combining the road map with Perl-based cross-attention and its efficacy in aligning generated data with real observations. Additionally, Method (a)→(c) results in marked improvements of 9.59% in mAP, 7.99% in NDS, 0.14% in mAOE and 3.80% in Vehicle mIoU, strongly supporting the utility of Perl-based cross-attention in producing accurate data-annotation alignments for objects. To optimally regulate elements of the background and foreground, Method (c), in contrast to baseline Method (a), indicates increases of 8.62% in mAP, 8.16% in NDS, 0.16% in mAOE, 0.52% in Road mIoU and 4.66% in Vehicle mIoU. These results validate the efficiency of Perl-based cross-attention in enhancing image controllability.

Effectiveness of Masking Map Weight Coefficients. Tab. 5 examines the effects of varying masking map weight coefficients λ_s and λ_b , where higher weights indicate greater integration of Perl knowledge into network learning. The table demonstrates that the detection metrics improve with increasing values of λ_s and λ_b , while the FID score increases, underscoring the significant role of Perl knowledge in the controllable learning process of the diffusion model. For optimal controllability of the generative model, we set the default values of λ_s and λ_b to 5.0 in the main paper.

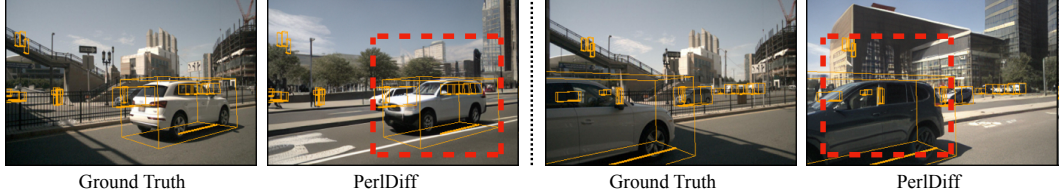


Figure 6: Failure cases of our PerlDiff, with red markers highlighting instances where, compared to the ground truth, our PerlDiff generates images with the front and rear of vehicles reversed.

Qualitative Visualization. We assess the efficacy of our PerlDiff against the baseline BEVControl*, with both approaches aimed at synthesizing perspective scene images. As illustrated in Fig. 1, PerlDiff generates images of substantially superior quality compared to the baseline, especially in the accurate depiction of object orientations, positions, and sizes. More results can be found in the Appendix D.

5 Conclusion

In conclusion, our PerlDiff introduces a streamlined framework that adeptly merges geometric constraints with synthetic street view image generation, harnessing diffusion models’ power for high-fidelity visuals. The architecture boasts a Perl-based controlling module (Perl-CM) that, through training, becomes seamlessly integrated with Stable Diffusion. Meanwhile, a cutting-edge Perl-based cross-attention mechanism guarantees meticulous feature guidance at the object level for precise control. Experiments on NuScenes [1] and KITTI [7] datasets confirm our PerlDiff’s enhanced performance in image synthesis and downstream tasks like 3D object detection and segmentation. Flexible yet precise, our PerlDiff’s method of Perl-based cross-attention with geometric perspective projections during training finely balances image realism with accurate condition alignment.

Limitation and Future Work. Fig. 6 depicts several failure cases of our PerlDiff, where the model erroneously generates vehicles with the front and rear orientations reversed, in contrast to the ground truth. This limitation arises from the usage of a Perl mask in our PerlDiff, which does not account for the orientation on the 2D Perl plane. Future endeavors may explore video generation, extending to work such as DrivingDiffusion [12], Panacea [36], and Driving into the Future [35].

References

- [1] Caesar, H., Bankiti, V., Lang, A.H., Vora, S., Lioung, V.E., Xu, Q., Krishnan, A., Pan, Y., Baldan, G., Beijbom, O.: nuscenes: A multimodal dataset for autonomous driving. In: Proceedings of the IEEE/CVF conference on computer vision and pattern recognition. pp. 11621–11631 (2020)
- [2] Choi, J., Kim, S., Jeong, Y., Gwon, Y., Yoon, S.: Ilvr: Conditioning method for denoising diffusion probabilistic models. arXiv preprint arXiv:2108.02938 (2021)
- [3] Couairon, G., Careil, M., Cord, M., Lathuilière, S., Verbeek, J.: Zero-shot spatial layout conditioning for text-to-image diffusion models. In: Proceedings of the IEEE/CVF International Conference on Computer Vision. pp. 2174–2183 (2023)
- [4] Dhariwal, P., Nichol, A.: Diffusion models beat gans on image synthesis. Advances in neural information processing systems **34**, 8780–8794 (2021)
- [5] Esser, P., Rombach, R., Ommer, B.: Taming transformers for high-resolution image synthesis. In: Proceedings of the IEEE/CVF conference on computer vision and pattern recognition. pp. 12873–12883 (2021)
- [6] Gao, R., Chen, K., Xie, E., Hong, L., Li, Z., Yeung, D.Y., Xu, Q.: Magicdrive: Street view generation with diverse 3d geometry control. arXiv preprint arXiv:2310.02601 (2023)
- [7] Geiger, A., Lenz, P., Urtasun, R.: Are we ready for autonomous driving? the kitti vision benchmark suite. In: Conference on Computer Vision and Pattern Recognition (CVPR) (2012)

- [8] Heusel, M., Ramsauer, H., Unterthiner, T., Nessler, B., Hochreiter, S.: Gans trained by a two time-scale update rule converge to a local nash equilibrium. *Advances in neural information processing systems* **30** (2017)
- [9] Ho, J., Jain, A., Abbeel, P.: Denoising diffusion probabilistic models. *Advances in neural information processing systems* **33**, 6840–6851 (2020)
- [10] Ho, J., Salimans, T.: Classifier-free diffusion guidance. *arXiv preprint arXiv:2207.12598* (2022)
- [11] Hong, S., Lee, G., Jang, W., Kim, S.: Improving sample quality of diffusion models using self-attention guidance. In: *Proceedings of the IEEE/CVF International Conference on Computer Vision*. pp. 7462–7471 (2023)
- [12] Li, X., Zhang, Y., Ye, X.: Drivingdiffusion: Layout-guided multi-view driving scene video generation with latent diffusion model. *arXiv preprint arXiv:2310.07771* (2023)
- [13] Li, Y., Liu, H., Wu, Q., Mu, F., Yang, J., Gao, J., Li, C., Lee, Y.J.: Glichen: Open-set grounded text-to-image generation. In: *Proceedings of the IEEE/CVF Conference on Computer Vision and Pattern Recognition*. pp. 22511–22521 (2023)
- [14] Li, Z., Wang, W., Li, H., Xie, E., Sima, C., Lu, T., Qiao, Y., Dai, J.: Bevformer: Learning bird's-eye-view representation from multi-camera images via spatiotemporal transformers. In: *European conference on computer vision*. pp. 1–18. Springer (2022)
- [15] Liu, Z., Tang, H., Amini, A., Yang, X., Mao, H., Rus, D.L., Han, S.: Bevfusion: Multi-task multi-sensor fusion with unified bird's-eye view representation. In: *2023 IEEE international conference on robotics and automation (ICRA)*. pp. 2774–2781. IEEE (2023)
- [16] Liu, Z., Mao, H., Wu, C.Y., Feichtenhofer, C., Darrell, T., Xie, S.: A convnet for the 2020s. In: *Proceedings of the IEEE/CVF conference on computer vision and pattern recognition*. pp. 11976–11986 (2022)
- [17] Loshchilov, I., Hutter, F.: Decoupled weight decay regularization. *arXiv preprint arXiv:1711.05101* (2017)
- [18] Mildenhall, B., Srinivasan, P.P., Tancik, M., Barron, J.T., Ramamoorthi, R., Ng, R.: Nerf: Representing scenes as neural radiance fields for view synthesis. *Communications of the ACM* **65**(1), 99–106 (2021)
- [19] Mou, C., Wang, X., Xie, L., Wu, Y., Zhang, J., Qi, Z., Shan, Y., Qie, X.: T2i-adapter: Learning adapters to dig out more controllable ability for text-to-image diffusion models. *arXiv preprint arXiv:2302.08453* (2023)
- [20] Nguyen-Phuoc, T., Li, C., Theis, L., Richardt, C., Yang, Y.L.: Hologan: Unsupervised learning of 3d representations from natural images. In: *Proceedings of the IEEE/CVF International Conference on Computer Vision*. pp. 7588–7597 (2019)
- [21] Niemeyer, M., Geiger, A.: Giraffe: Representing scenes as compositional generative neural feature fields. In: *Proceedings of the IEEE/CVF Conference on Computer Vision and Pattern Recognition*. pp. 11453–11464 (2021)
- [22] Qu, L., Wu, S., Fei, H., Nie, L., Chua, T.S.: Layoutllm-t2i: Eliciting layout guidance from llm for text-to-image generation. In: *Proceedings of the 31st ACM International Conference on Multimedia*. pp. 643–654 (2023)
- [23] Radford, A., Kim, J.W., Hallacy, C., Ramesh, A., Goh, G., Agarwal, S., Sastry, G., Askell, A., Mishkin, P., Clark, J., et al.: Learning transferable visual models from natural language supervision. In: *International conference on machine learning*. pp. 8748–8763. PMLR (2021)
- [24] Rombach, R., Blattmann, A., Lorenz, D., Esser, P., Ommer, B.: High-resolution image synthesis with latent diffusion models. In: *Proceedings of the IEEE/CVF conference on computer vision and pattern recognition*. pp. 10684–10695 (2022)

[25] Ronneberger, O., Fischer, P., Brox, T.: U-net: Convolutional networks for biomedical image segmentation. In: *Medical Image Computing and Computer-Assisted Intervention–MICCAI 2015: 18th International Conference, Munich, Germany, October 5–9, 2015, Proceedings, Part III* 18. pp. 234–241. Springer (2015)

[26] Sohl-Dickstein, J., Weiss, E., Maheswaranathan, N., Ganguli, S.: Deep unsupervised learning using nonequilibrium thermodynamics. In: *International conference on machine learning*. pp. 2256–2265. PMLR (2015)

[27] Song, J., Meng, C., Ermon, S.: Denoising diffusion implicit models. *arXiv preprint arXiv:2010.02502* (2020)

[28] Song, Y., Garg, S., Shi, J., Ermon, S.: Sliced score matching: A scalable approach to density and score estimation. In: *Uncertainty in Artificial Intelligence*. pp. 574–584. PMLR (2020)

[29] Song, Y., Sohl-Dickstein, J., Kingma, D.P., Kumar, A., Ermon, S., Poole, B.: Score-based generative modeling through stochastic differential equations. *arXiv preprint arXiv:2011.13456* (2020)

[30] Swerdlow, A., Xu, R., Zhou, B.: Street-view image generation from a bird’s-eye view layout. *IEEE Robotics and Automation Letters* (2024)

[31] Taud, H., Mas, J.: Multilayer perceptron (mlp). *Geomatic approaches for modeling land change scenarios* pp. 451–455 (2018)

[32] Van Den Oord, A., Vinyals, O., et al.: Neural discrete representation learning. *Advances in neural information processing systems* **30** (2017)

[33] Voynov, A., Aberman, K., Cohen-Or, D.: Sketch-guided text-to-image diffusion models. In: *ACM SIGGRAPH 2023 Conference Proceedings*. pp. 1–11 (2023)

[34] Wang, S., Liu, Y., Wang, T., Li, Y., Zhang, X.: Exploring object-centric temporal modeling for efficient multi-view 3d object detection. *arXiv preprint arXiv:2303.11926* (2023)

[35] Wang, Y., He, J., Fan, L., Li, H., Chen, Y., Zhang, Z.: Driving into the future: Multiview visual forecasting and planning with world model for autonomous driving. *arXiv preprint arXiv:2311.17918* (2023)

[36] Wen, Y., Zhao, Y., Liu, Y., Jia, F., Wang, Y., Luo, C., Zhang, C., Wang, T., Sun, X., Zhang, X.: Panacea: Panoramic and controllable video generation for autonomous driving. *arXiv preprint arXiv:2311.16813* (2023)

[37] Xie, J., Li, Y., Huang, Y., Liu, H., Zhang, W., Zheng, Y., Shou, M.Z.: Boxdiff: Text-to-image synthesis with training-free box-constrained diffusion. In: *Proceedings of the IEEE/CVF International Conference on Computer Vision*. pp. 7452–7461 (2023)

[38] Yang, K., Ma, E., Peng, J., Guo, Q., Lin, D., Yu, K.: Bevcontrol: Accurately controlling street-view elements with multi-perspective consistency via bev sketch layout. *arXiv preprint arXiv:2308.01661* (2023)

[39] Zhang, L., Rao, A., Agrawala, M.: Adding conditional control to text-to-image diffusion models. In: *Proceedings of the IEEE/CVF International Conference on Computer Vision*. pp. 3836–3847 (2023)

[40] Zhang, Y., Lu, J., Zhou, J.: Objects are different: Flexible monocular 3d object detection. In: *Proceedings of the IEEE/CVF Conference on Computer Vision and Pattern Recognition*. pp. 3289–3298 (2021)

[41] Zhou, B., Krähenbühl, P.: Cross-view transformers for real-time map-view semantic segmentation. In: *Proceedings of the IEEE/CVF conference on computer vision and pattern recognition*. pp. 13760–13769 (2022)

The supplementary material is organized into the following sections:

- Section **A**: DDPM Preliminaries
- Section **B**: Implementation Details
- Section **C**: Additional Experiments
- Section **D**: Visualization Results

A DDPM Preliminaries

Denoising Diffusion Probabilistic Models (DDPM) [9] are a class of generation models which simulate a Markov chain of diffusion steps to gradually convert data samples into pure noise. The generative process is then reversed to synthesize new samples from random noise. We commence with an observation x_0 sampled from the data's true distribution $q(x)$, and then progressively apply Gaussian noise over a series of T time steps. The forward diffusion is mathematically defined as $q(x_t|x_{t-1}) = \mathcal{N}(x_t; \sqrt{1 - \beta_t}x_{t-1}, \beta_t\mathbf{I})$, where β_t is a variance term that can be either time-dependent or learned during training. The entire forward diffusion process can be represented as the product of the conditional distributions from each step:

$$q(x_{1:T}|x_0) = \prod_{t=1}^T q(x_t|x_{t-1}), \quad (7)$$

where the sequence $\{\beta_t\}_{t=1}^T$ specifies the noise schedule applied at each timestep. The diffusion process is notable for permitting direct sampling of x_t from x_0 using a closed-form expression:

$$q(x_t|x_0) = \sqrt{\bar{\alpha}_t}x_0 + \sqrt{1 - \bar{\alpha}_t}\epsilon, \quad \text{where } \epsilon \sim \mathcal{N}(0, \mathbf{I}), \quad (8)$$

in which $\alpha_t = 1 - \beta_t$ and the cumulative product $\bar{\alpha}_t = \prod_{s=1}^t \alpha_s$. To synthesize new samples, a reverse process known as the backward diffusion is learned, which conceptually undoes the forward diffusion. This inverse transition is captured through a parameterized Gaussian distribution:

$$p_\theta(x_{t-1}|x_t) = \mathcal{N}(x_{t-1}; \mu_\theta(x_t), \sigma_\theta^2(x_t)\mathbf{I}). \quad (9)$$

B Implementation Details

Our PerlDiff utilize the pre-trained Stable Diffusion v1.4 [24], augmented with specific modifications to enhance scene control. Training was executed on a server equipped with eight Tesla V100 (32 GB) GPUs, across 60,000 iterations. An initial batch size of 16 was adjusted to a per-GPU batch of two for focused optimization, particularly for data samples comprising six view images per frame. The generation of samples conforms to the CFG rule [10], employing a guidance scale of 5.0 and the Denoising Diffusion Implicit Models (DDIM) [27] across 50 steps.

For scene manipulation, the text encoder within Stable Diffusion is retained, along with a weight-frozen CLIP to manage textual inputs and ConvNext for processing road maps. Feature extraction from Perl boxes is conducted via an MLP, optimized through Perl-based controlling module (Perl-CM) with randomly initialized weights. In contrast, certain modules inherit and freeze pre-trained weights from Stable Diffusion v1.4. The key parameters within Perl-CM, λ_b and λ_s , are set to 5.0 to facilitate optimal image synthesis. Furthermore, DDIM [27] and CFG [10] are integrated into our training regimen, with a novel approach of omitting all conditions at a rate 10% to foster model versatility.

Optimization employs AdamW [17], without weight decay coefficient and a learning rate of 5×10^{-5} , complemented by a warm-up strategy in the first 1,000 iterations. For additional insight into the realm of autonomous driving models, BEVFormer [14], StreamPETR [34], and CVT [41] were re-trained with original configurations tailored to our target resolution. The performance of BEVFusion [15] and MonoFlex [40] was evaluated using their provided codes and pre-trained weights.

C Additional Experiments

In this section, we present additional experiments conducted to validate controllability at different resolutions (256×704) and to assess the contributions of individual components within our PerlDiff. Our studies focus on the following aspects:

- Effectiveness of Controllable Generation on NuScenes (Subsection C.1)
- Effectiveness of Classifier-Free Guidance Scale (Subsection C.2)
- Effectiveness of View Cross-attention for Multi-View Consistency (Subsection C.3)

Our results confirm the superior performance of our method across various resolutions and illustrate how each component is integral to the success of our PerlDiff.

C.1 Effectiveness of Controllable Generation on NuScenes

In Tab. 6, we conduct a comparative analysis to emphasize the capabilities of PerlDiff for controllable generation at a resolution of 256×704 . This quantitative evaluation contrasts our method with other leading approaches based on the detection metrics provided by BEVFusion [15]. Our PerlDiff exhibits significantly superior performance, achieving mAP improvements of 3.84% and 11.50%, and NDS increases of 0.45% and 10.80%, compared to MagicDrive [6] and BEVControl*, respectively. These results confirm the efficacy of PerlDiff in the precise controllable generation at the object level.

Table 6: Controllability comparison for street view image generation on the NuScenes [1] validation set. A quantitative evaluation using 3D object detection metrics from BEVFusion [15].

Method	FID \downarrow	mAP \uparrow	NDS \uparrow	mATE \downarrow	mASE \downarrow	mAOE \downarrow
Oracle	–	35.54	41.20	0.67	0.27	0.56
MagicDrive [6]	16.59	20.85	30.26	–	–	–
BEVControl*	27.14	13.19	19.91	0.94	0.34	0.96
PerlDiff (Ours)	26.61	24.69	30.71	0.82	0.28	0.76

C.2 Effectiveness of Classifier-Free Guidance Scale

In Tab. 7, we assess the effect of the CFG [10] scale on the sampling of data generation. The term “scale” refers to the CFG scale, which is adjusted to balance conditional and unconditional generation. The transition from Method (b) to (e) indicates an increase in the CFG scale from 5.0 to 12.5. The results show an average increase of 2.60 in FID, an average decrease of 0.87% in mAP, an average reduction of 1.03% in NDS, a 0.02% increase in mAOE and a 1.07% drop in Vehicle mIoU. This provides substantial evidence that an excessively large CFG scale can degrade the quality of generated images and adversely affect various performance metrics.

Table 7: Comparison of different CFG [10] scale to each metric. We report the 3D object detection results based on BEVFormer [14] and BEV Segmentation results based on CVT [41].

Method	scale	FID \downarrow	mAP \uparrow	NDS \uparrow	mAOE \downarrow	Road mIoU \uparrow	Vehicle mIoU \uparrow
Oracle	–	–	27.06	41.89	0.54	70.35	33.36
(a)	2.5	22.95	23.89	36.03	0.70	60.05	26.95
(b)	5.0	25.06	25.10	36.24	0.72	61.26	27.13
(c)	7.5	26.70	24.62	35.60	0.74	61.52	26.63
(d)	10.0	27.78	24.20	35.05	0.73	61.43	26.00
(e)	12.5	28.51	23.86	34.98	0.74	61.25	25.55

C.3 Effectiveness of View Cross-attention for Multi-View Consistency

View cross-attention ensures the seamless integration of visual data by maintaining continuity and consistency across the multiple camera feeds that are integral to current multi-functional perception systems in autonomous vehicles. Typically, autonomous vehicles feature a 360-degree horizontal surround view from a BEV perspective, resulting in overlapping fields of vision between adjacent cameras. Consequently, we facilitate direct interaction between the noise maps of each camera and those of the immediate left and right cameras. Given the noisy images from the current, left, and

right cameras, designated as \mathbf{Z}_{in} , \mathbf{Z}_l , and \mathbf{Z}_r , respectively, the output of this multi-view generation is given by:

$$\mathbf{Z} = \mathbf{Z}_{in} + \mathcal{C}(\mathbf{Z}_{in}, \mathbf{Z}_l, \mathbf{Z}_l) + \mathcal{C}(\mathbf{Z}_{in}, \mathbf{Z}_r, \mathbf{Z}_r), \quad (10)$$

where $\mathcal{C}(\cdot)$ represents the standard cross-attention operation, which accepts three input parameters: query, key, and value, respectively. This approach systematically integrates spatial information from various viewpoints, enabling the synthesis of images that exhibit visual consistency across distinct camera perspectives. Fig. 7 offers a visual comparison of the model output with and without the application of view cross-attention.



Figure 7: Comparative visualization of outputs with (left) and without (right) view cross-attention. Red markers highlight discontinuities in the images generated without view cross-attention.

D Visualization Results

To further showcase the controllable generation capabilities of our PerlDiff, we present additional visual results. Fig. 8 provides extended examples of manipulating object orientation and size, while Fig. 9 demonstrates the precision of the model in positional control.

Comparative visualizations, as illustrated in Fig. 10, reveal that while BEVControl* produces chaotic and indistinct attention maps leading to suboptimal image quality, our PerlDiff optimizes the response areas of the attention map, resulting in accurate object-level control information.

Additionally, Fig. 11 displays scene alterations by PerlDiff to mimic different weather conditions or times of day, showcasing its versatility in changing scene descriptions. Besides, Fig. 12 exhibits a series of synthetic samples generated with NuScenes *validation* set, showcasing the method’s adaptability and robustness in a variety of urban scenarios. Furthermore, Fig. 13 presents samples from KITTI [7] *validation* set, illustrating the application’s performance in real-world conditions.



Figure 8: Visualization of controlling object **orientation** and **size**. We present the results of our PerlDiff and BEVControl* in terms of controlling the orientation and size of objects. From top to bottom, the orientation of the object increases incrementally (-60° , 60° , and 90°), and from left to right, we display objects of different sizes (car, truck, and bus).



Figure 9: Visualization of controlling object **position**. We present the results of PerlDiff and BEVControl* in terms of controlling the position of objects. From left to right, the objects progressively move forward, and from top to bottom, we display objects of varying sizes (car, truck, and bus).

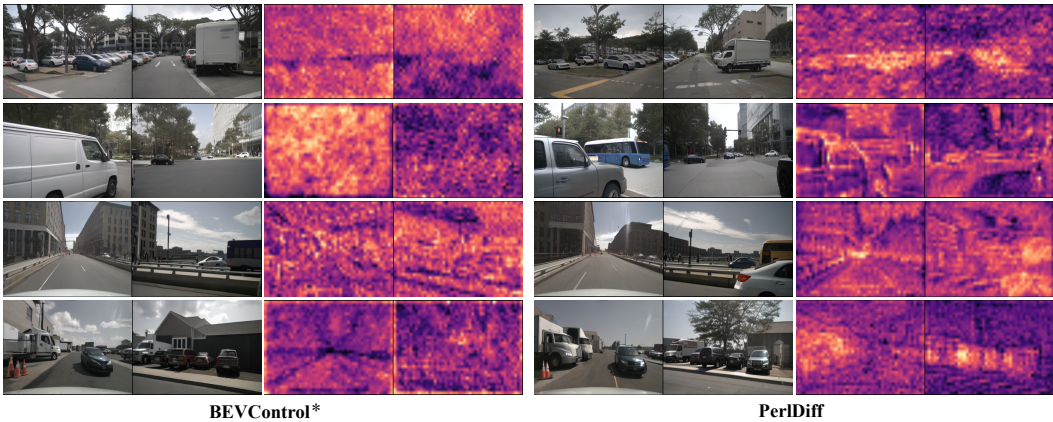


Figure 10: Visualization of cross-attention map results. From left to right, we present the generated images and corresponding cross-attention maps from our baseline BEVControl* and our PerlDiff.

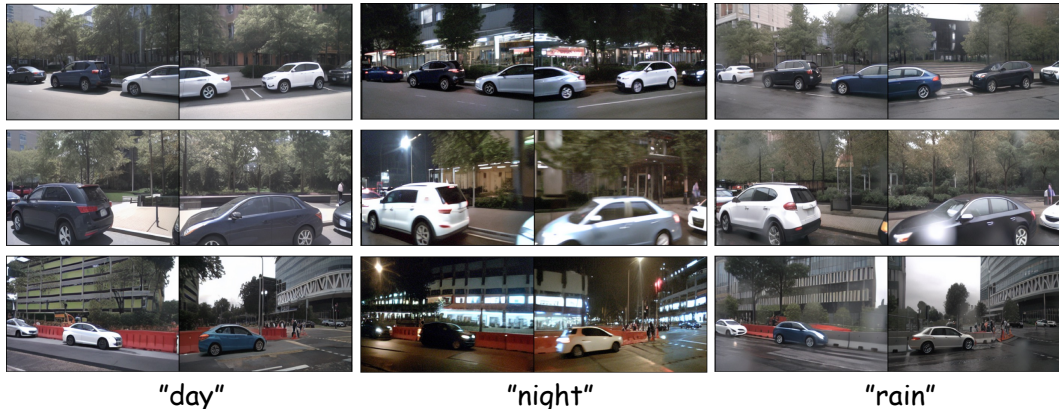


Figure 11: Qualitative visualizations on NuScenes [1]: *day*, *night*, and *rain* scenarios synthesized by our PerlDiff, exhibiting adaptability to various lighting and weather conditions.

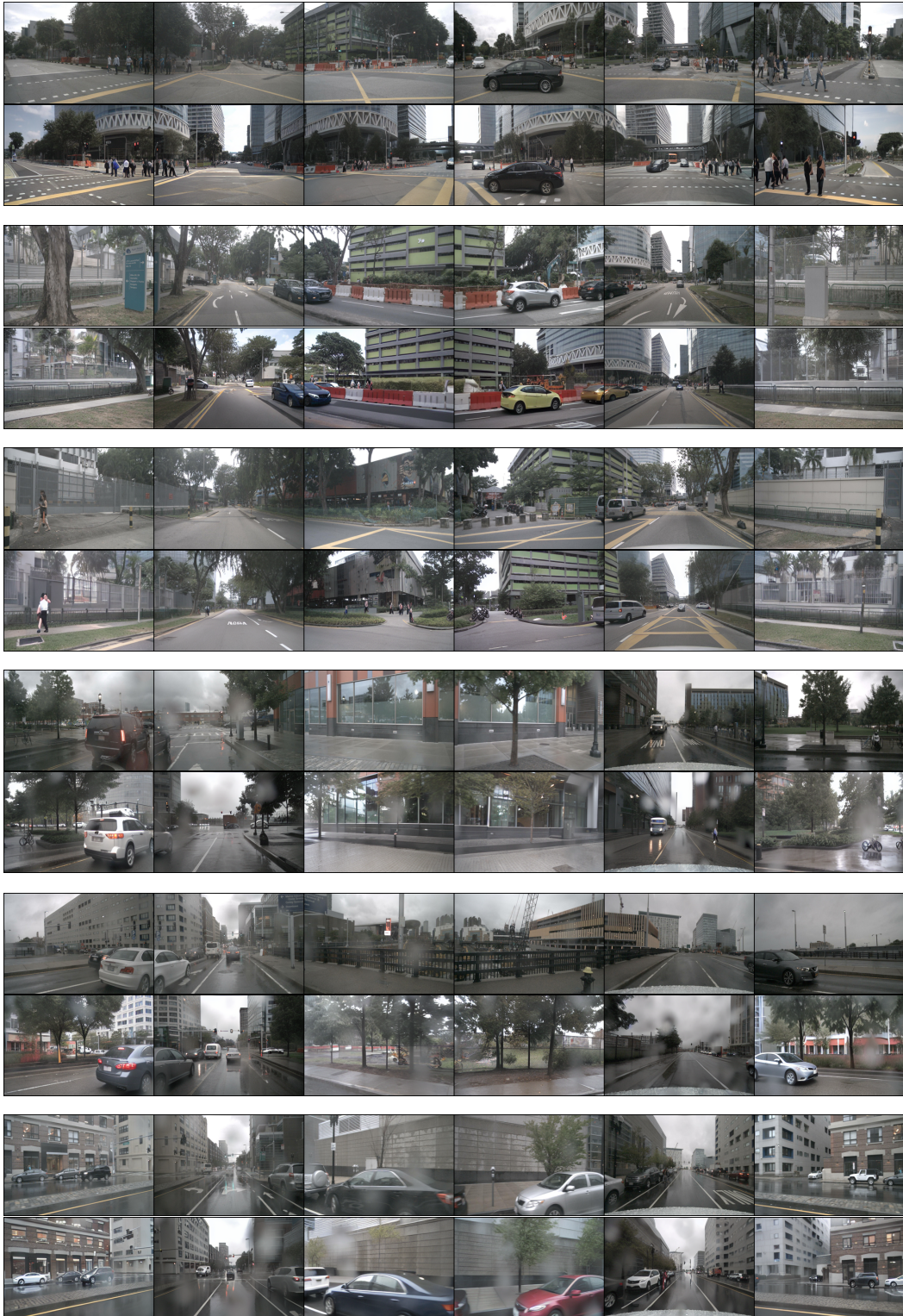


Figure 12: Visualization of street view images generated by our PerlDiff on NuScenes [1] validation dataset. We show the ground truth (1st row) and our PerlDiff (2nd row).



Figure 13: Visualization of street view images generated by our PerlDiff on KITTI [7] validation dataset. We show the ground truth (left) and our PerlDiff (right).